https://doi.org/10.1016/j.envpol.2021.117648

Title

Improved Raman spectroscopy-based approach to assess microplastics in seafood

Authors

Matthew Ming-Lok Leung[a], Yuen-Wa Ho[a], Cheng-Hao Lee[a,b], Youji Wang[c], Menghong Hu[c], Kevin Wing-Hin Kwok[a,d], Song-Lin Chua[a,d], James Kar-Hei Fang[a,d]*

Affiliations

[a] Department of Applied Biology and Chemical Technology, The Hong Kong Polytechnic University, Kowloon, Hong Kong SAR, China

[b] Institute of Textiles and Clothing, The Hong Kong Polytechnic University, Kowloon, Hong Kong SAR, China

[c] International Research Centre for Marine Biosciences, Shanghai Ocean University, Nanhui New City, Shanghai, China

[d] Research Institute for Future Food, The Hong Kong Polytechnic University, Kowloon, Hong Kong SAR, China

*Corresponding author: james.fang@polyu.edu.hk

Keywords

Fish, mussels, Raman mapping, autofluorescence, food contamination

Abstract

Microplastics represent an emerging environmental issue that have been found almost everywhere including seafood, raising a great concern about the ecological and human health risks they pose. This study addressed the common technical challenges in the assessment of microplastics in seafood by developing an improved protocol based on Raman spectroscopy and using the green-lipped mussel *Perna viridis* and the Japanese jack mackerel *Trachurus japonicus* as the test models. Our findings evaluated a type of stainless-steel filter membranes with minimal Raman interference, and a combination of chemicals that achieved 99–100% digestion efficiency for both organic and inorganic biomass. This combined chemical treatment reached 90–100% recovery rates for seven types of microplastics, on which the surface modification was considered negligible and did not affect the accuracy of polymer identification based on Raman spectra, which showed 94–99% similarity to corresponding untreated microplastics. The developed extraction method for microplastics was further combined with an automated Raman mapping approach, from which our results confirmed the presence of microplastics in *P. viridis* and *T. japonicus* collected from Hong Kong waters. Identified microplastics included polypropylene, polyethylene, polystyrene and poly(ethylene terephthalate), mainly in the form of fragments and fibres. Our protocol is applicable to other biological samples, and provides an improved alternative to streamline the workflow of microplastic analysis for routine monitoring purposes.

Graphical Abstract

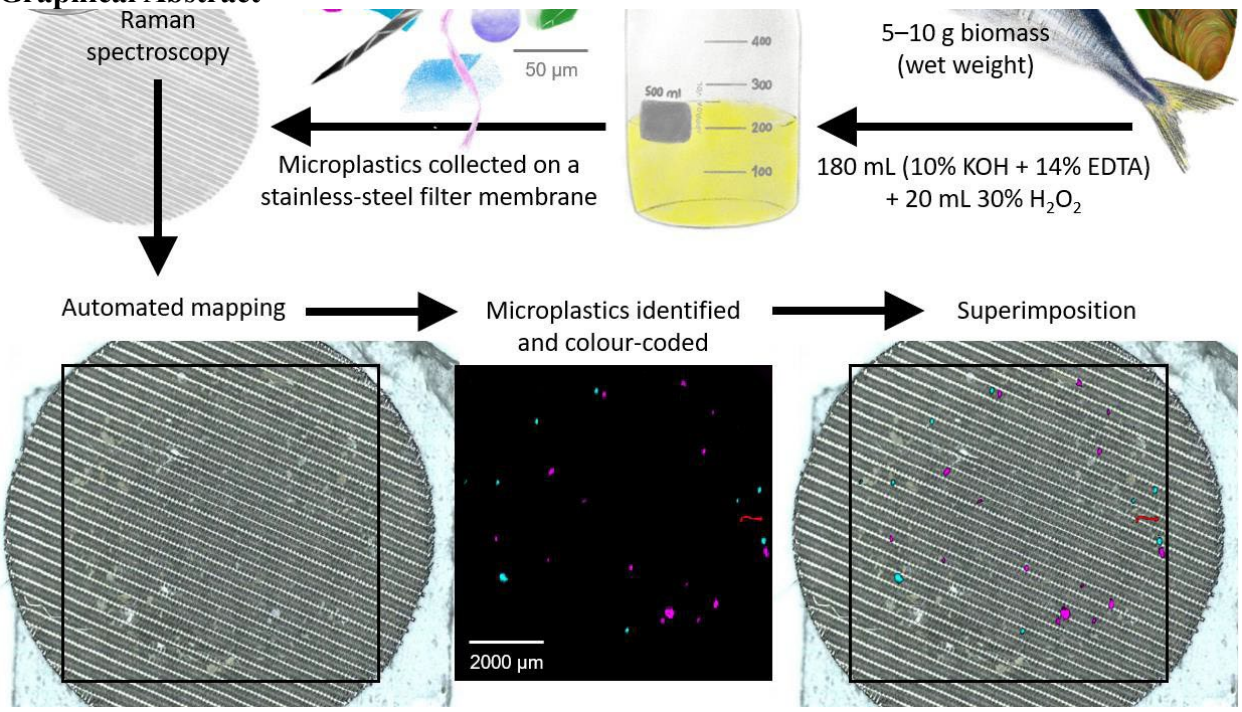

Introduction

The annual global production rate of plastics has exceeded 359 million metric tons, among which 250 million metric tons may end up as waste in the ocean by 2025 (Katija et al., 2017; Plastics Europe, 2019). Plastic debris in the marine environment can be broken into microplastics, i.e. plastic pieces that are less than 5,000 μm long, through photochemical oxidation and other degradation processes (Andrady, 2011). Microplastics have raised great ecological concerns due to their increasing prevalence and harmful effects when ingested by marine organisms, such as blockage of the digestive tract, impaired predatory performance, bioaccumulation of these plastic particles and their trophic transfer along food chains (de Sá et al., 2015; Jovanović, 2017). A lot of these marine organisms are seafood items, which provide a route for microplastics to enter the human diet. There are numerous studies reporting microplastics in marine organisms, ranging from polychaetes to higher trophic-level fish including seafood species (Van Cauwenberghe et al., 2015; Collard et al., 2017; Cho et al., 2019; Hossain et al., 2020). However, the various analytical approaches and criteria adopted by different researchers have made data comparison among studies difficult (Qiu et al., 2016). Analysis of microplastics generally comprises the following four steps, each of which however holds its own limitations.

Biomass digestion – Biological samples should be digested as much as possible to extract microplastics. Otherwise, autofluorescence of the biomass would create strong interference in the analysis of microplastics using Raman spectroscopy, one of the most widely used analytical techniques in plastic polymer research (Xiong et al., 2018; Karbalaei et al., 2019; James et al., 2020). A number of acidic and alkaline solutions are used for this purpose, among which the performance of diluted potassium hydroxide (KOH) appears to be more satisfactory (Avio et al., 2015a; Dehaut et al., 2016; Karami et al., 2017). The digestion effectiveness of KOH can be further boosted by the combined use with an oxidising agent such as hydrogen peroxide (H_2O_2) or sodium hypochlorite (Teng et al., 2019; Gündoğdu et al., 2020). However, the use of these chemicals or their combination may damage microplastics. For instance, nitric acid has been found to dissolve some plastic polymers such as polyamine and is not recommended for the analysis of microplastics (Roch and Brinker, 2017). It is therefore important to assess the impacts of selected chemicals on the integrity of microplastics in each biomass digestion protocol.

Density separation – The common biomass digestion protocols may not be completely effective to remove the inorganic contents in biomass such as fish bones or the mantle of bivalve shellfish (Bonello et al., 2018; Garnier et al., 2019; Bagheri et al., 2020). In this regard, a separation step in a dense medium is often used to float and separate microplastics of lower density from inorganic biomass and other abiotic matter (Claessens et al., 2013; Phuong et al., 2018; Hossain et al., 2020). The commonly used dense media include solutions of sodium chloride, sodium iodide, sodium tungstate and zinc chloride at 1.2–1.5 g mL^{-1} (Dehaut et al., 2016; Qu et al., 2018;, Karbalaei et al., 2019; Nie et al., 2019). However, these density levels are incapable of floating some of the high-density microplastics such as polytetrafluoroethylene. To address this concern, the present study explored an alternative approach using a solution of ethylenediaminetetraacetic acid (EDTA) to digest inorganic biomass and bypass the need of the density separation step. EDTA is commonly used in decalcification of bones and in this study was added in the biomass digestion step to remove both organic and inorganic contents in seafood samples (Bancroft and Gamble, 2008).

Retrieval of microplastics – Microplastics suspended in solution after the biomass digestion or density separation step are often retrieved on a filter membrane as the substrate platform to facilitate characterisation of microplastics, e.g. using Raman spectroscopy (Gündoğdu et al., 2020). The selected filter membranes should have pore sizes smaller than the target size range of microplastics, and should not generate any significant noise to the Raman signals of samples. Filter membranes made of glass fibres or cellulose esters are commonly available in marine biology and food laboratories, but these materials show strong interference in the Raman fingerprint region of plastic polymers and are thus not ideal for microplastic analysis. In this regard, we evaluated the use of filter membranes made of stainless steel, a form of iron-chromium-nickel alloys which is less sensitive to Raman excitation that may serve as a more suitable substrate for microplastic analysis.

Characterisation of microplastics – Earlier studies relied on visual inspection to identify and describe microplastics, a process that can achieve approximately 70% accuracy by trained analysts but is however prone to overestimation (Directive, 2013; Verlaan et al., 2019). The later development using Raman or Fourier-transform infrared (FTIR) spectroscopy has substantially improved the reliability of microplastic analysis, but the workflow still requires visual screening to sort out suspected microplastics to be analysed one by one. The step of visual screening is time-consuming and can be subjective and prone to handling errors. This concern can be addressed by adopting an automated mapping approach, a function that is available in some latest models of Raman or FTIR spectroscopes to locate and identify the polymer types, sizes and shapes of microplastics over a specified area on the filter substrate (Löder et al. 2015; Käppler et al. 2016; Sobhani et al., 2019, 2020; Xu et al. 2019; Levermore et al., 2020). Here, we provided an application example of using automated Raman mapping technology to streamline the workflow of microplastic analysis.

In view of the above limitations and suggested solutions, this study aimed to develop an improved protocol for assessing microplastics in seafood samples based on Raman spectroscopy. Five objectives were set to achieve this aim (Fig. 1). The first two objectives were centred around method optimisation: Objective 1 was to identify a filter substrate with minimal Raman interference and, while in Objective 2 we tested different chemical treatments to increase the biomass digestion efficiency, particularly for the inorganic contents which are common in marine biological samples. Objective 3 and Objective 4 were used to evaluate the effects of these digestion chemicals on microplastics in terms of particle recovery and surface modification, respectively. The developed protocol was furthermore tested in Objective 5 for its combined application with a Raman mapping approach. The evaluation was performed on two popular seafood species in the Indo-Pacific region, namely the green-lipped mussel *Perna viridis*, also a widely used species for pollution biomonitoring, and the Japanese jack mackerel *Trachurus japonicus*, which represents a commercially important fishery resource in the region (Kim et al., 2016; Sun et al., 2020).

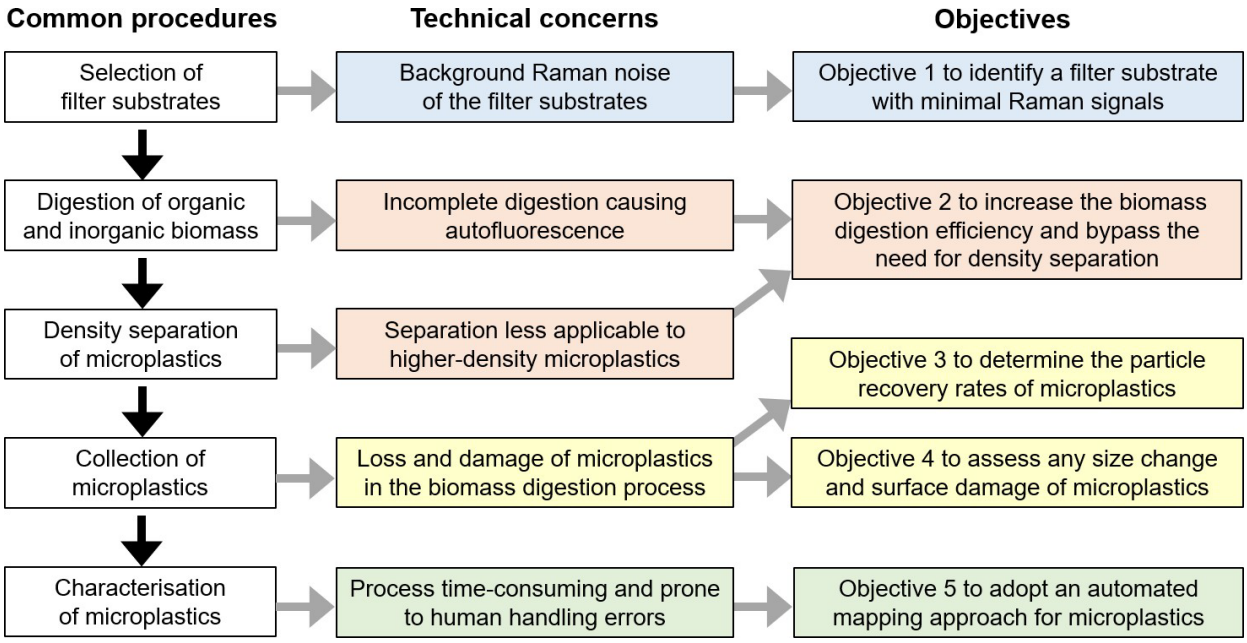

Fig. 1. Five objectives of the present study using a Raman spectroscopy-based approach to address common technical concerns in the extraction and analysis of microplastics from biological samples including seafood.

Materials and methods

Two sources of interference are common in the Raman spectroscopy-based assessment of microplastics, namely the background Raman noise due to the substrate materials, and autofluorescence due to the sample biological matrices. The first part of this study addressed the two issues by identifying a type of filter substrate with minimal response to Raman excitation (Objective 1), and by developing a modified method to maximise biomass digestion efficiency (Objective 2).

Objective 1: selecting a filter substrate suitable for Raman spectrometry

Three types of filter membranes made of glass fibres (Valusep, Thomas Scientific, Swedesboro, NJ), cellulose esters (Advantec, Tokyo, Japan) and stainless steel (Xinmingde Machinery, Henan, China) were used. Their performance as Raman substrate was evaluated using polystyrene (PS) of three particle sizes (300, 100 and 10 µm) in a 3 × 3 factorial experimental design leading to nine treatments (n = 5). The 300 and 100 µm PS particles were cryogenically ground from PS standard pellets (Acros Organics, Fair Lawn, NJ) using a Retsch CryoMill (Haan, Germany). The pre-cooling stage lasted 7 min at 5 shakes s^{-1}, followed by a grinding stage for 1.5 min at 25 shakes s^{-1} at –196 °C. The ultra-low temperature was maintained by liquid nitrogen circulating outside the grinding chamber made of zirconium oxide. Ground particles of ca. 300 and 100 µm in the longest dimension were handpicked for the experiment. The 10 µm PS was supplied by Polysciences (Warrington, PA).

Five particles of each size of PS were added on each type of substrate, dried at 40 °C and assessed with a Renishaw inVia confocal Raman spectroscope (Wotton-under Edge, UK) equipped with a Leica 10× objective (NA = 0.25; Wetzlar, Germany) and a 785 nm diode laser source (300 mW output power). Raman spectra of the PS particles were acquired in the

wavenumber range of 676–1767 cm^{-1} using 10% laser power and 5 s exposure time. Baseline correction and smoothing of the acquired spectra were performed with the Renishaw WiRE 5.2 software. All sample spectra were compared with the reference Raman spectrum of PS provided in the Renishaw Polymeric Materials Database. The similarity of each sample spectrum to the reference spectrum was indicated by the matching index provided in WiRE 5.2 (range: 0–1), an estimate which served as the tested variable among the nine treatments. A lower value of the index indicated a greater interference by the substrate material on identification of microplastics.

Objective 2: assessing biomass digestion efficiency

P. viridis (mussel shell length of ca. 80 mm) and *T. japonicus* (fish fork length of ca. 200 mm) were provided by local fishermen in August 2019 and stored at –20 °C. For experimental use, *P. viridis* was thawed to extract the whole soft tissue from the shells, while thawed *T. japonicus* was cut into pieces containing bones. The mussel and fish samples were blot-dried, wet-weighed and thoroughly rinsed with Milli-Q water (Merck, Darmstadt, Germany) prior to the digestion process. Sample wet weights are summarised in Table 1. With these biomass samples, we tested the digestion efficiency of KOH (Acros Organics) in combination with H_2O_2 (Sigma Aldrich, St. Louis, MO) and EDTA (Acros Organics). The experimental approach formed a 2 × 3 factorial design (n = 5), in which two species of biomass (*P. viridis* and *T. japonicus*) were tested across three combinations of chemicals (K, KH and KHE; Table 1). All solutions were prepared with Milli-Q water and filtered through 0.22 μm before use. Our goal was to develop a digestion protocol suitable for both organic and inorganic biomass including mussel mantles and fish bones.

Table 1. Six biomass digestion treatments in Objective 2 for the green-lipped mussel *Perna viridis* and the Japanese jack mackerel *Trachurus japonicus*, using three combinations of potassium hydroxide (KOH), hydrogen peroxide (H_2O_2) and ethylenediaminetetraacetic acid (EDTA). Tested biomass was measured in wet weight (mean ± SD; n = 5).

Treatment	Digestion solutions (200 mL at 40 ºC for 48 h)	Sample wet weight (g)
P. viridis		
K	200 mL 10% KOH	6.88 ± 0.73
KH	180 mL 10% KOH, added with 20 mL 30% H_2O_2	6.39 ± 0.76
KHE	180 mL 10% KOH and 14% EDTA, added with 20 mL 30% H_2O_2	6.88 ± 0.63
T. japonicus		
K	200 mL 10% KOH	4.89 ± 0.18
KH	180 mL 10% KOH, added with 20 mL 30% H_2O_2	5.30 ± 0.23
KHE	180 mL 10% KOH and 14% EDTA, added with 20 mL 30% H_2O_2	5.11 ± 0.29

The mussel and fish biomass samples were digested at 40 ºC for 48 h in treatments K, KH and KHE. The ratio of digestion volume (mL) to sample wet weight (g) was higher than 20:1. In treatment K, 200 mL of 10 % KOH was used throughout the digestion process. Treatment KH was started with 180 mL of 10 % KOH, with 10 mL of 30% H_2O_2 added twice at 24 h and 42 h to make the final volume to 200 mL. Treatment KHE was further modified from treatment KH, whose initial 180 mL solution contained 10 % KOH and 14 % EDTA. The solution after digestion was filtered through a pre-weighed filter membrane (stainless steel; pore size: 30 μm) to retain undigested biomass, if any. Each filter membrane that was coated with biomass was dried at 40 °C and reweighed. This dry weight minus the membrane pre-weight equalled the dry weight of the undigested biomass. The ratio of undigested biomass to initial biomass revealed the digestion inefficiency of each treatment, which when subtracted by one, yielded the digestion

efficiency. The initial biomass was only available in wet weight and was converted into dry weight to facilitate the calculation. Additional 200 pieces of *P. viridis* soft tissue (ca. 0.6 g each) and 100 pieces of *T. japonicus* (ca. 5 g each) were blot-dried, wet-weighed, rinsed, dried at 40 °C and weighed again. The weight conversion factors for *P. viridis* and *T. japonicus* were estimated from the corresponding ratios of dry weight to wet weight.

The above work in Objective 1 and Objective 2 resolved the technical issues related to Raman interference that were caused by filter substrate and biomass materials. Treatment KHE, which used the stainless-steel filter membranes, was identified as a suitable approach to extract microplastics from the mussel and fish biomass (see Results). The second part of this study determined how this approach would affect the characterisation of microplastics using Raman spectrometry in terms of particle recovery (Objective 3) and surface modification (Objective 4).

Objective 3: determining particle recovery rates of microplastics

Seven types of microplastics, polypropylene (PP), polyethylene (PE), polystyrene (PS), polyamine 6/6 (PA), poly(methyl methacrylate) (PMMA), poly(ethylene terephthalate) (PET) and poly(vinyl chloride) (PVC), were used in the evaluation. The required microplastics were made with a cryogenic grinder as in Objective 1. The plastic materials were sourced from domestic products, except for PE and PS, which were standard pellets supplied by Maoming Petrochemical (Guangzhou, China) and Acros Organics, respectively. The mean particle sizes of these microplastics ranged from 412 to 648 μm (Table 2).

Table 2. Summary of the microplastics made by cryogenic grinding and their particle sizes, expressed as the longest diameter (mean ± SD; n = 10).

Microplastics made	Density (g mL^{-1})*	Particle size (μm)	Plastic source
Polypropylene (PP)	0.85–0.92	566 ± 99	PP food containers
Polyethylene (PE)	0.89–0.97	601 ± 131	PE standard pellets
Polystyrene (PS)	1.04–1.09	412 ± 67	PS standard pellets
Polyamine 6/6 (PA)	1.12–1.15	508 ± 79	Nylon cable ties
Poly(methyl methacrylate) (PMMA)	1.16–1.20	535 ± 88	Acrylic sheets
Poly(ethylene terephthalate) (PET)	1.38–1.41	648 ± 125	PET egg cartons
Poly(vinyl chloride) (PVC)	1.16–1.41	564 ± 92	PVC pipes

*The values of density provided by Stuart (2002) and Nakajima and Yamashita (2020)

Table 3. Five treatments of KHE in Objective 3 to evaluate the extraction recovery of microplastics from ca. 5 g biomass of *Perna viridis* and *Trachurus japonicus*. The spike recovery tests accounted for the background microplastics in the tested biomass. Refer to Table 1 for the KHE treatment conditions and Table 2 for the abbreviations of microplastics.

KHE digestion treatment	Spiked microplastics	Evaluation
Chemicals only + microplastics	PP, PE, PS, PA, PMMA, PET and PVC	Recovery of microplastics
P. viridis biomass	Nil	Background microplastics
P. viridis biomass + microplastics	PP, PE, PS, PA, PMMA, PET and PVC	Recovery of microplastics*
T. japonicus biomass	Nil	Background microplastics
T. japonicus biomass + microplastics	PP, PE, PS, PA, PMMA, PET and PVC	Recovery of microplastics*

*Background microplastics in the corresponding biomass to be subtracted in the calculation of recovery rates

The evaluation consisted of five treatments of KHE (Table 3; n = 5). In the treatment with chemicals only, ten particles of each type of microplastics (10 × 7 = 70 particles; Table 2) were spiked into the KHE solution and subject to the same digestion process as in Objective 2, after

which the microplastics were retrieved on a stainless-steel filter membrane (pore size: 30 μm). The numbers and polymer types of these microplastics were determined using Raman spectroscopy as in Objective 1. The recovery rate of each type of microplastics was expressed as the retrieved number to spiked number ratio.

For the other treatments with biomass, mussel and fish samples were individually homogenised with a DLAB D-160 handheld homogeniser (Beijing, China). Each homogenate was divided into two portions with similar wet weights. The seven types of microplastics were spiked into one of the portions, while the other portion served as a control to determine the background microplastics in the biomass. These pairs of spiked portion and control portion of *P. viridis* and *T. japonicus* formed the four KHE treatments with biomass (Table 3). Microplastics were extracted and identified from these biomass treatments, as in the chemicals-only treatment. The number of retrieved microplastics in the spiked portion, minus that in the control portion, divided by the spiked number yielded the recovery rate of each type of microplastics.

Objective 4: evaluating surface modification of microplastics

Chemically-induced modification on microplastics due to treatment KHE, if any, was investigated in terms of surface damage (changes in microtopography), particle size (changes in surface area), and whether these changes would affect the accuracy of polymer identification (changes in Raman characteristic peaks).

Scanning electron microscopy was used to assess the surface microtopography of microplastics. Selected particles after treatment KHE in Objective 3, along with intact untreated microplastics, were coated with a 10–20 nm layer of gold by a Nanoimages MCM-200 ion sputter coater (Pleasanton, CA). Surface features of these microplastics, KHE-treated or untreated, were observed and compared at an acceleration voltage of 20 kV using a Tescan Vega3 scanning electron microscope (Brno, Czech Republic).

To quantify changes in surface area, the seven types of microplastics (n = 5; Table 2) were mounted on glass slides with an epoxy putty (Henco, Taizhou, China), a process that fixed the orientation and exposed the surface of each particle throughout the experiment. The whole slides mounted with microplastics were immersed in the KHE solution without biomass and subject to the same digestion process as in Objective 2, before and after which the exposed surfaces of all microplastics were individually scanned at a resolution of 2 μm using a Keyence VK-X200 3D laser scanning microscope (Osaka, Japan; see Fig. 5a). The area of interest was set to be the exposed surface of each microplastic mounted on the epoxy putty to assess the effects of KHE. Moreover, Raman spectra were acquired from these microplastics before and after the digestion process, using the same settings as in Objective 1 in the wavenumber range of 100–3200 cm^{-1}. The similarity between the initial and final Raman peak profiles were determined based on their ratio of matching index. A lower ratio indicated a greater influence of treatment KHE on identification of microplastics.

Objective 5: adopting an automated mapping approach in microplastic monitoring

Findings from Objective 3 and Objective 4 confirmed the usefulness of our improved microplastic extraction protocol, which showed > 99% digestion efficiency for biomass and > 90% recovery rates for all tested microplastics with minimal damage that can be clearly

identified in Raman spectroscopy (see Results). The last part of this study was to combine this protocol with a Raman mapping approach, in which microplastics > 30 μm on a specified area were mapped and characterised by an automated programme to reduce human handling errors.

The soft tissue of *P. viridis* (n = 3) and whole fish of *T. japonicus* (n = 3), collected from the eastern waters of Hong Kong in August 2019, were digested in the KHE solution as in Objective 2. The solution after digestion was filtered through stainless-steel filter membranes with pore sizes of 250 μm (straight weave) and then 30 μm (plain Dutch weave) to separate two size ranges of microplastics, i.e. > 250 μm and 30–250 μm. Raman spectra of microplastics > 250 μm were acquired using the point-measurement approach as in Objective 1. The polymer types were identified using the Renishaw Polymeric Materials Database. Raman spectra of microplastics of 30–250 μm were acquired using an automated mapping approach, in which the whole area coated with microplastics (8 mm × 8 mm) on each filter membrane was scanned and mapped at a spatial resolution of 28.4 μm and acquisition time of 5 s per pixel. Other parameters remained the same as in Objective 1. This mapping process required approximately 14 h and produced more than 10,000 Raman spectra per sample, among which microplastics were identified using the Renishaw Polymeric Materials Database. The identified microplastics were colour-coded and illustrated in a two-dimensional panel, from which microplastics were characterised in terms of their abundance, particle size, polymer type, and shape. The morphology of the identified microplastics was confirmed under a Cossim XTZ-7075A stereomicroscope (Beijing, China).

Statistical analysis

Data obtained from the factorial designed experiments in Objective 1 (3 types of filter membranes × 3 particle sizes of PS) and Objective 2 (2 species of biomass × 3 groups of chemicals in biomass digestion) were tested by two-way analysis of variance (ANOVA), in which the Raman matching index of PS and biomass digestion efficiency served as the tested variables, respectively. The data violated the Shapiro-Wilk test for normality, or homogeneity of variance, and were aligned rank-transformed using ARTool (Wobbrock et al. 2011). If interaction was significant between the two factors in two-way ANOVA, then the effect of each factor was tested by a Kruskal-Wallis test and, if significant, followed by Dunn's multiple comparisons. In Objective 4, changes in surface area were tested for each type of microplastics before and after treatment KHE using a dependent *t*-test, in which data transformation was not required. The above statistical procedures were carried out using SPSS Statistics 25.0 (IBM, Armonk, NY).

Results

Objective 1: selecting a filter substrate suitable for Raman spectroscopy

Raman spectra of the tested filter membranes were acquired at 785 nm excitation. The glass-fibre membranes displayed a broad band that centred around 1400 cm^{-1}, while major peaks at around 900, 1300 and 1400 cm^{-1} were identified from the membranes made of cellulose esters. However, the stainless-steel membranes appeared to be insensitive to Raman excitation with no observable peaks (Fig. 2a). The interference of using these filter membranes as the substrate materials in Raman spectroscopy on identification of microplastics was tested with PS of three particle sizes.

The matching index, which indicated the accuracy of polymer identification, was compared among the different types of filter membranes and PS particle sizes (Fig. 2b–c). Significant

interaction between the two factors was detected in two-way ANOVA on aligned rank-transformed data (F (4, 36) = 12.52, $p < 0.001$). The effects of filter membrane on changes in matching index of PS were then compared at each particle size class. The index values ranged from 0.86 ± 0.03 to 0.97 ± 0.07 for the 100 and 300 µm PS on different filter membranes, respectively, and no significant differences were detected among these values in respective Kruskal-Wallis tests ($p = 0.06$ and 0.37). However, when the particle size of PS decreased to 10 µm, the use of stainless-steel filter membranes resulted in significantly higher index values (0.43 ± 0.11) compared to glass fibres (0.00 ± 0.00) and cellulose esters (0.06 ± 0.13) in Kruskal-Wallis tests followed by Dunn's multiple comparisons ($p < 0.01$ and 0.05, respectively; Fig. 2b). Given its lower interference on PS identification, stainless steel was identified as a more suitable material of filter membranes for the Raman spectroscopy-based analysis of microplastics.

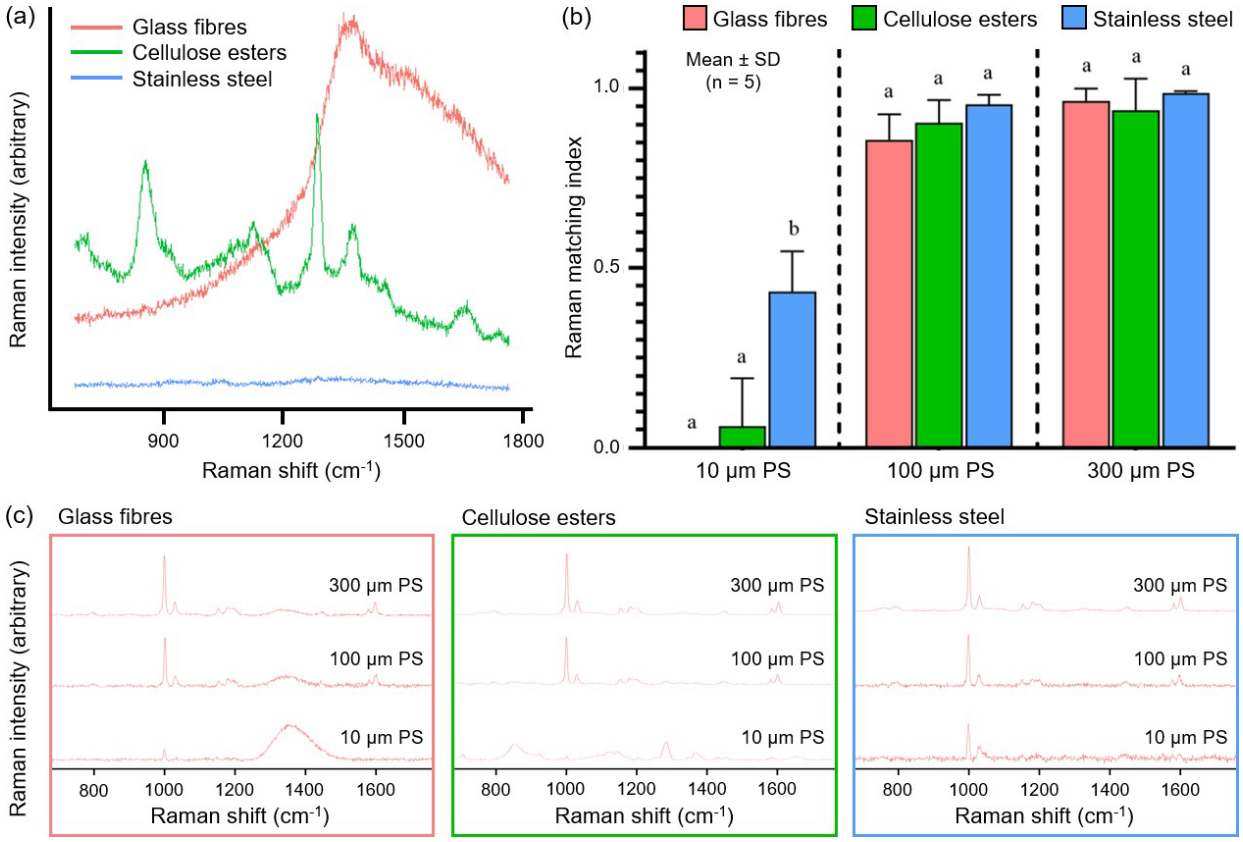

Fig. 2. (a) Raman spectra of filter membranes made of glass fibres, cellulose esters and stainless steel excited at 785 nm; (b) Raman matching index of polystyrene (PS), determined for three particle sizes (10, 100 and 300 µm) and placed on the three types of filter membranes presented in (a). The index ranged from 0 to 1, of which a higher value indicated a greater similarity of the sample spectrum to the reference Raman spectrum. Significant interaction (filter membrane × particle size) was detected in two-way ANOVA on aligned rank-transformed data ($p < 0.05$). Kruskal-Wallis test and Dunn's multiple comparisons were used to compare the effects of filter membranes on each particle size of PS. Significant differences were detected at 10 µm PS and indicated by different lower-case letters ($p < 0.05$). (c) Raman spectra of PS of the three particle sizes placed on the three materials excited at 785 nm using a 10× objective (NA = 0.25). It

should be noted that the matching index of 10 μm PS on stainless steel (0.43 ± 0.11) can be increased to 0.94 ± 0.01 (n = 5) when using a 50× objective (NA = 0.75).

Objective 2: assessing biomass digestion efficiency

The biomass digestion efficiency of treatments K, KH and KHE was determined on the whole soft tissue of mussels (*P. viridis*) and fish pieces with bones (*T. japonicus*) in terms of the percentage change in biomass dry weight. A significant interaction between the factors of treatment and biomass was detected in two-way ANOVA on aligned rank-transformed data (F (2, 24) = 20.742, $p < 0.001$). The effects of the three treatments were then separately compared for the mussel and fish biomass. The digestion efficiency on mussel biomass ranged from 99.9 ± 0.13% to 100 ± 0.01%, which did not lead to any significant changes among the three treatments ($p = 0.15$, Kruskal-Wallis test; Fig. 3a). Although no significant changes in digestion efficiency were revealed in the calculation based on dry weight, the stereomicrographs showed a clear reduction in the amount of undigested mussel biomass in treatment KHE than that in treatments K or KH (Fig. 3b).

As for the fish biomass, only 74.7 ± 9.79% and 76.6 ± 6.72% were digested in treatments K and KH, respectively. A large number of undigested biomass, which was mostly fish bones, remained after the two treatments (Fig. 3c). Nevertheless, the fish digestion efficiency increased to 99.9 ± 0.19% in treatment KHE, which was significantly higher than that in treatment K ($p < 0.05$, Kruskal-Wallis tests followed by Dunn's multiple comparisons; Fig. 3a). According to these findings from mussel and fish biomass, treatment KHE was selected as a more suitable digestion method and its influence on the extraction process of microplastics was evaluated in Objectives 3 and 4.

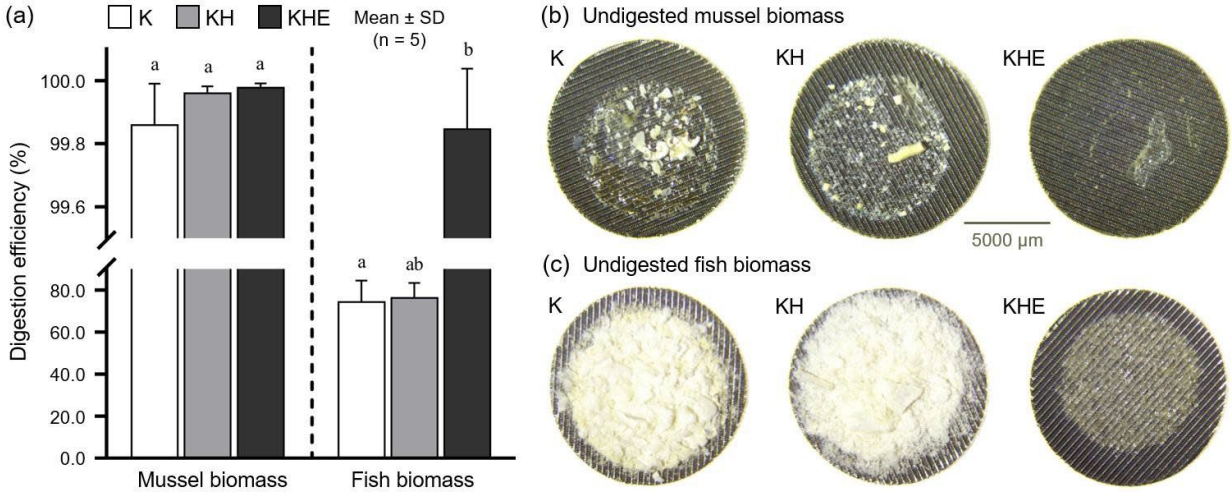

Fig. 3. (a) Biomass digestion efficiency of *Perna viridis* and *Trachurus japonicus* in treatments K, KH and KHE. The treatment conditions are provided in Table 1. Significant interaction (treatment × biomass) was detected in two-way ANOVA on aligned rank-transformed data ($p < 0.05$). Kruskal-Wallis test and Dunn's multiple comparisons were used to compare the three treatment at each species of biomass. The treatment effects were found to be significant on the fish biomass, as indicated by different lower-case letters ($p < 0.05$); (b) stereomicrographs of undigested biomass of *P. viridis* and (c) *T. japonicus* retained on stainless-steel filter membranes

(pore size: 30 μm) after treatments K, KH and KHE. All panels in (b) and (c) share the same scale bar.

Objective 3: determining particle recovery rates of microplastics

Seven types of microplastics were spiked in treatment KHE with and without biomass, after which the spiked particles were retrieved on stainless-steel filter membranes and identified based on Raman spectra (Fig. 4). It was confirmed that the tested biomass did not contain any background microplastics. The spike recovery rates of microplastics were summarised in Table 4, of which the mean values in the chemical-only treatment (90–100%) were similar to those with the mussel biomass (92–100%) and fish biomass (90–98%). These findings showed the effectiveness of treatment KHE to extract microplastics from biomass in terms of particle number.

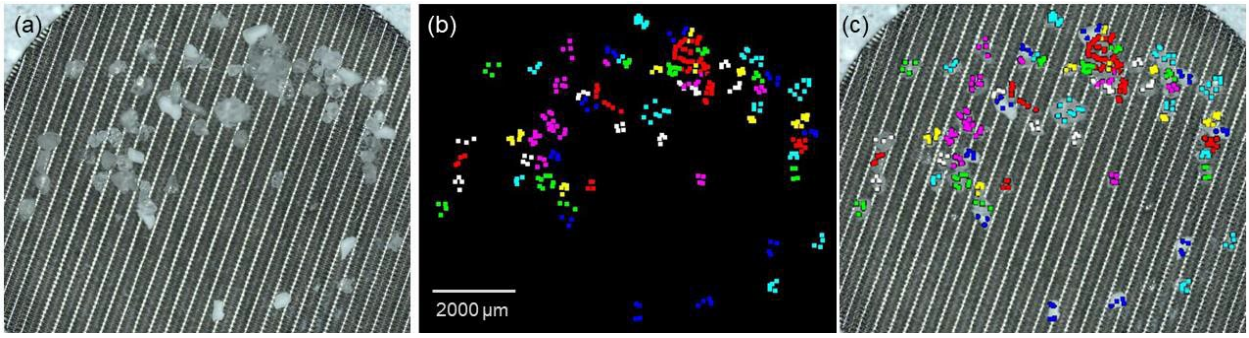

Fig. 4. (a) Microplastics retrieved on a stainless-steel filter membrane after the spike recovery test, (b) their identification using Raman spectroscopy in a point acquisition mode at 785 nm excitation, and (c) the superimposed image of (a) and (b). Retrieved microplastics were counted and identified to be PP (purple), PE (cyan), PS (yellow), PA (white), PMMA (green), PET (red) and PVC (blue). Refer to Table 2 for the abbreviations of microplastics. The coloured dots indicate the acquisition points of Raman spectra. Three or four spectra were acquired for each particle to verify the polymer type.

Table 4. Spike recovery rates (%) of microplastics in treatment KHE with and without biomass of *Perna viridis* and *Trachurus japonicus* (mean ± SD; n = 5). Refer to Table 1 for the KHE treatment conditions and Table 2 for the abbreviations of microplastics.

Treatment KHE	PP	PE	PS	PA	PMMA	PET	PVC
Chemicals only	100 ± 0.00	96.0 ± 5.48	98.0 ± 4.47	100 ± 0.00	96.0 ± 5.48	96.0 ± 5.48	90 ± 7.07
P. viridis biomass	94.0 ± 8.94	92.0 ± 4.47	96.0 ± 5.48	100 ± 0.00	98.0 ± 8.37	100 ± 0.00	96.0 ± 5.48
T. japonicus biomass	98.0 ± 8.37	96.0 ± 5.48	90.0 ± 7.07	96.0 ± 5.48	96.0 ± 5.48	96.0 ± 5.48	96.0 ± 5.48

Objective 4: evaluating surface modification of microplastics

Changes in surface area of microplastics due to treatment KHE were evaluated using 3D laser scanning technology (Fig. 5a). No significant changes were found in all types of microplastics except PP and PVC, of which the mean surface areas significantly increased by 16.2 ± 6.64% and 7.86 ± 4.03% after the treatment, respectively ($p < 0.05$, dependent *t*-test; Fig. 5b). Likewise, the scanning electron micrographs displayed similar microtopography between the KHE-treated

and untreated microplastics, but slightly more peeling was observed on some particles including PP after the treatment. Another observation was that the treated PVC was associated with crevices and pits on the surface (Fig. 6). Raman spectra of the microplastics were compared before and after treatment KHE. The spectra of all pairs were almost identical, reaching a similarity of 94–99% which revealed the minimal effect of treatment KHE on the accuracy of identifying microplastics despite the surface modification on PP and PVC (Fig. 7; Table 5).

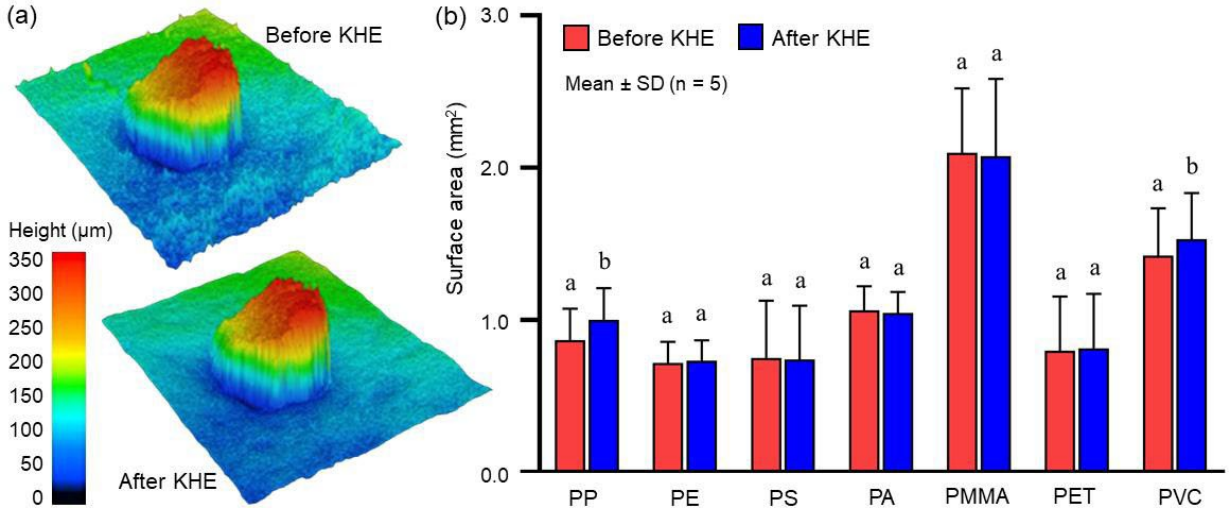

Fig. 5. (a) The surface area of a representative microplastic measured at a resolution of 2 µm using 3D laser scanning technology, before and after treatment KHE (see Table 1). The substrate layer was an epoxy putty to mount the microplastic on a glass slide; (b) changes in surface area of microplastics due to treatment KHE, determined as in (a). Significant increases were detected for PP and PVC in respective dependent *t*-tests, and indicated by letters a and b ($p < 0.05$). Refer to Table 2 for the abbreviations of microplastics.

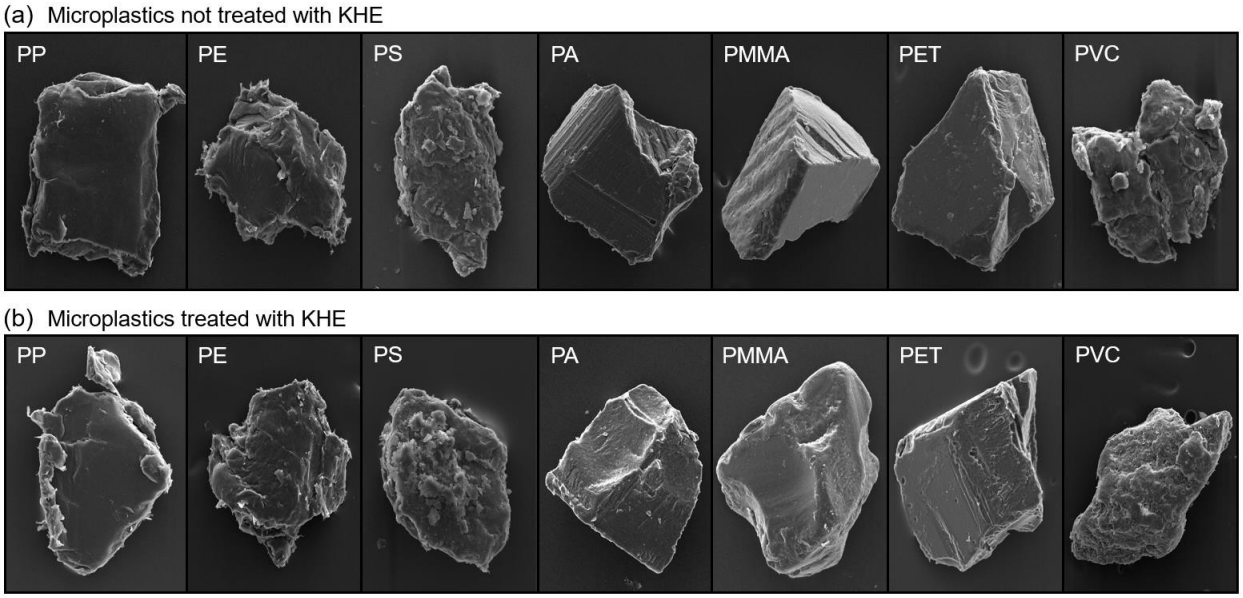

Fig. 6. Scanning electron micrographs of representative microplastics (a) not treated with KHE and (b) treated with KHE. The micrographs presented in (a) and (b) were produce from different

particles. Sizes of the displayed particles were ca. 200–500 µm. Refer to Table 1 for the KHE treatment conditions and Table 2 for the abbreviations of microplastics.

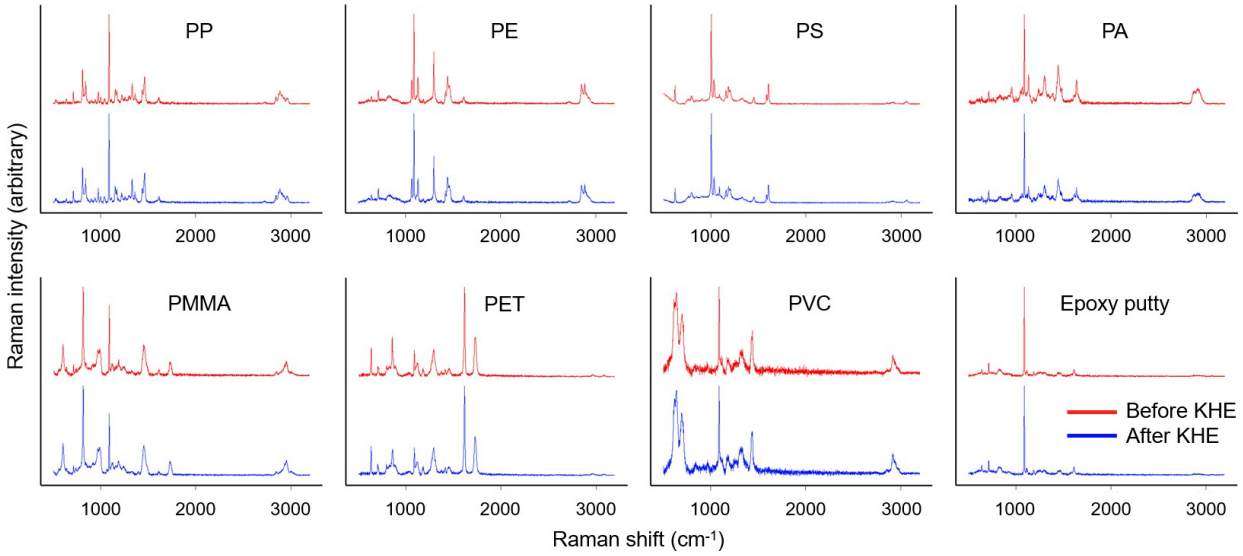

Fig. 7. Raman spectra of microplastics, and the epoxy putty used to mount microplastics (see Fig. 5), before and after treatment KHE (see Table 1). Raman spectra were acquired at 785 nm excitation. Refer to Table 2 for the abbreviations of microplastics.

Table 5. Similarity (%) between the Raman spectra of microplastics before and after treatment KHE reported in Fig. 7, as indicated by the ratio of matching index (mean ± SD; n = 5). Refer to Table 2 for the abbreviations of microplastics.

PP	PE	PS	PA	PET	PMMA	PVC
98.8 ± 1.79	94.4 ± 3.91	93.8 ± 3.77	95.2 ± 3.49	99.0 ± 0.71	99.0 ± 1.00	95.2 ± 4.55

Objective 5: adopting an automated mapping approach in microplastic monitoring

The developed extraction method for microplastics using stainless-steel filter membranes and treatment KHE was combined with a Raman mapping technique to characterise microplastics in seafood samples (Fig. 8). *P. viridis* and *T. japonicus* were used in this evaluation, where 32.7 ± 29.3 and 8.33 ± 7.09 pieces of microplastics per individual were found in the mussel soft tissue and whole fish, respectively (Fig. 9a), values that were equivalent to 4.46 ± 3.72 and 0.26 ± 0.16 per g wet weight in the mussels and fish. The particle size ranges of the identified microplastics were 38.2–820 µm and 67.7–805 µm, respectively, in the mussels and fish in terms of the longest dimension (Fig. 9a).

The microplastics were dominated by fragments, accounting for 97.6% and 80.0% in the mussels and fish, respectively, followed by fibres (Fig. 9b, 10). As for the polymer types, 82.7% of the microplastics extracted from mussels were confirmed to be PP, followed by PE (16.3%) and PET (1.02%). The highest proportion of PP (32.0%) was also found among the microplastics in fish, of which the polymer types were more diverse also including PS (28.0%), PE (24.0%), PET (12.0%) and PMMA (4.00%; Fig. 9c). These findings confirmed the presence of microplastics in seafood in Hong Kong.

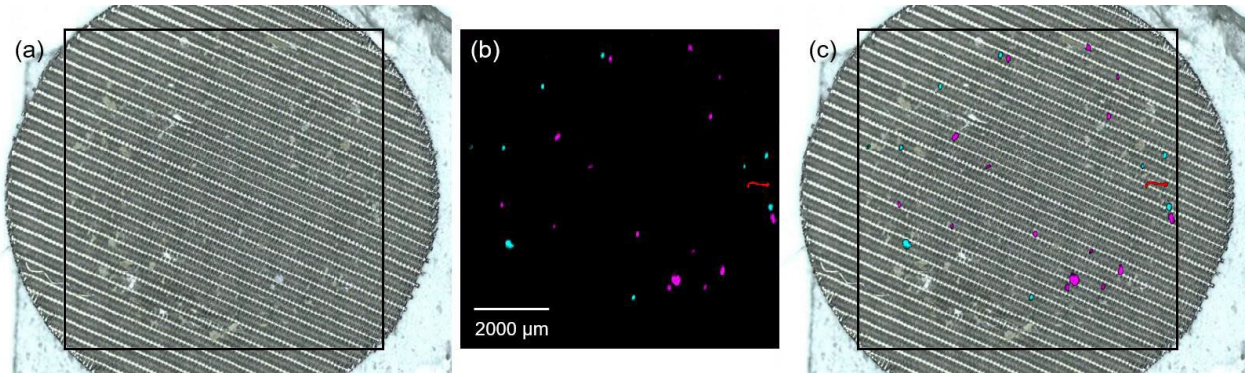

Fig. 8. (a) Microplastics on a stainless-steel filter membrane, (b) their colour-coded identification using an automated Raman mapping approach, and (c) the superimposed image of (a) and (b). All particles including microplastics within the black square were scanned and mapped at a spatial resolution of 28.4 µm, where polypropylene (pink), polyethylene (cyan) and poly(ethylene terephthalate) (red) were found in this sample.

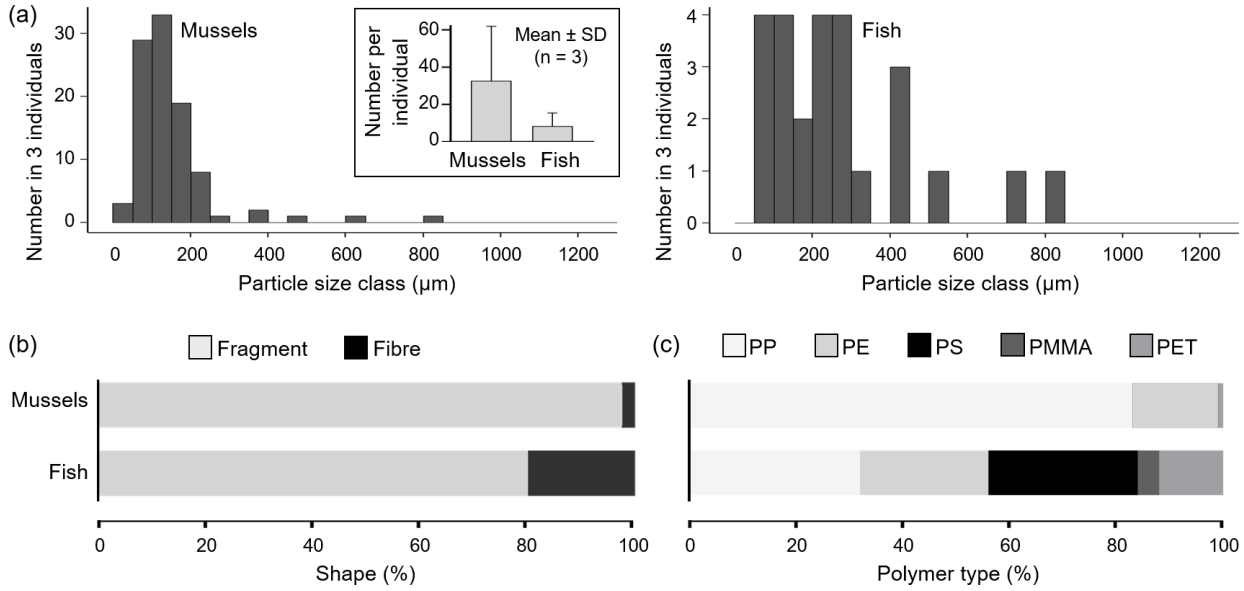

Fig. 9. (a) Number and particle size range of microplastics identified in *Perna viridis* (ca. 80 mm shell length) and *Trachurus japonicus* (ca. 200 mm total length), and the proportional distribution of microplastics in terms of (b) shape and (c) polymer type.

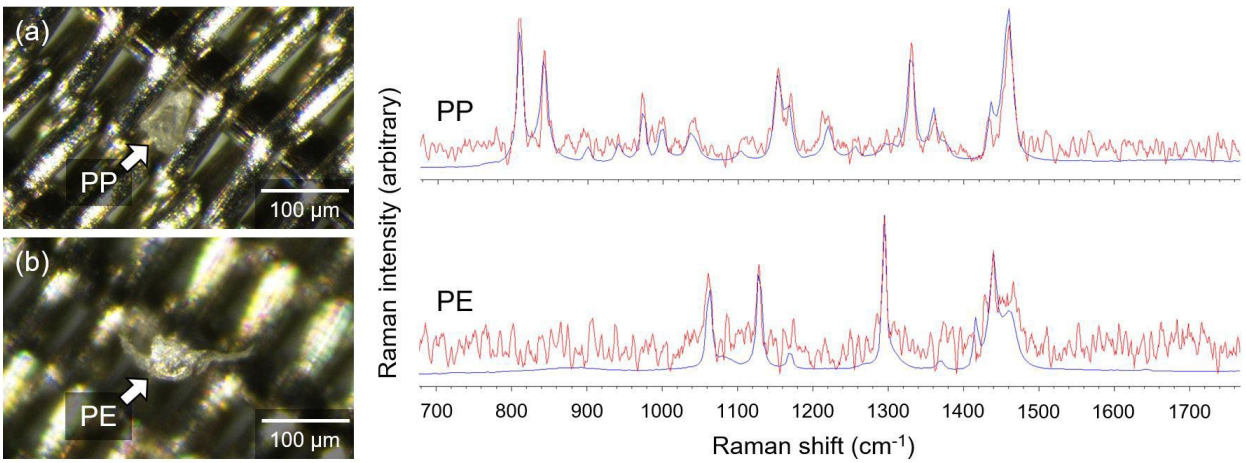

Fig. 10. Microplastic fragments extracted from (a) *Perna viridis* and (b) *Trachurus japonicus* and retained on stainless-steel filter membranes with a plain Dutch weave pattern. The two fragments were identified to be polypropylene (PP) and polyethylene (PE), respectively, by comparing their Raman spectra (red) to the reference spectra (blue).

Discussion

Stainless steel as a suitable substrate for Raman analysis

Filter membranes made of glass fibres and cellulose esters are widely used in the extraction of microplastics from biological and food samples (Hermabessiere et al., 2019; Gündoğdu et al., 2020; Sathish et al., 2020). However, these materials are sensitive to Raman excitation that can cause interference to the identification of microplastics. Our findings confirmed a strong fluorescence near 1400 cm^{-1} produced by the glass-fibre filter membranes when excited at 785 nm (Fig. 2a; Tuschel, 2016). The use of cellulose-ester filter membranes was associated with weaker fluorescence, but displayed distinct Raman bands in the region of 800–1400 cm^{-1} , which would overlap the characteristic peaks of common plastic polymers and hamper the identification of microplastics (see Fig. 7; Castro et al., 2011). This interference appeared to be size-dependent and was significant on 10 μm particles, which were not identifiable when the matching index reduced by up to 100% compared with the 100–300 μm particles (Fig. 2b, c).

Apart from glass fibres and cellulose esters, interference to Raman measurements was found to be common among filter membranes made of other materials. One possible solution to this issue is to coat a layer of Raman-insensitive materials such as aluminium on the filter membranes using electron beam evaporation (Oßmann et al., 2017). However, this surface modification process can be time-consuming and requires specific facilities and skilled personnel, requirements that may not be cost-effective for routine monitoring purposes. In this regard, the use of stainless steel can provide a low-cost option with satisfactory performance. In our study, the stainless-steel filter membranes produced minimal fluorescence and Raman excitation (Fig. 2a), and the highest matching index among all tested types (Fig. 2b, c; Lankers, 2019). It should be noted that the same 10× objective was used to fairly compare the Raman spectra obtained from PS across the size range of 10–300 μm on the three substrate materials. However, within the same laser spot size, a smaller particle is associated with a larger amount of background signal and therefore the Raman matching index is bound to be reduced. This issue can be addressed by using a higher-magnification objective, and that the matching index of 10 μm PS on stainless steel (0.43) can be increased to 0.94 on average under the same configuration but with a 50× objective.

Treatment KHE as an improved method to extract microplastics

This study tested the biomass digestion efficiency of KOH (treatment K) and attempted to improve its performance by adding H_2O_2 (treatment KH), and H_2O_2 with EDTA (treatment KHE; see Table 1). In line with earlier studies, treatment K and treatment KH were both effective in digesting organic matter, with almost 100% digestion efficiency achieved for the mussel biomass in terms of dry weight (Fig. 3a; Teng et al., 2019; Thiele et al., 2019; Zhang et al., 2020). However, a substantial amount of light-weighed undigested biomass was still observed after the treatments (Fig. 3b). The remaining biomass mainly comprised the inorganic content, e.g. in the mussel mantle, and could be associated with autofluorescence that interfered with Raman analysis. As for the fish samples, treatment K and treatment KH were less effective, leaving

behind > 20% undigested biomass including the inorganic content in fish bones (Fig. 3a). Likewise, in earlier studies, fish bones or inorganic substances that remained in the alimentary tract of fish were not fully digestible in KOH or H_2O_2 (Dehaut et al., 2016; Karami et al., 2017). Apart from the issue of autofluorescence, the relatively large amount of remaining biomass could easily clog the filter membranes and disrupt the extraction process of microplastics (Fig. 3b). In this regard, a density separation step could be used to isolate microplastics from the inorganic matter. However, the approach of density separation is less applicable for higher-density microplastics, potentially leading to the loss of these particles which should be avoided (Karami et al., 2017; Lusher et al., 2017).

Treatment KHE containing EDTA was developed to improve the biomass digestion efficiency and bypass the need of density separation. EDTA is a chelating agent used for gentle decalcification and was found useful here in digesting inorganic matter in the biomass, with almost 100% digestion efficiency achieved for both mussel and fish samples (Fig. 3a; Bancroft and Gamble, 2008). The amount of undigested biomass was dramatically reduced in treatment KHE, compared with treatment K and treatment KH (Fig. 3b). This approach was tested with seven types of microplastics and achieved high recovery rates of 90–100% (Table 4). However, slight peeling was observed on some of the particles after treatment KHE, an effect that might be associated with the increased surface area of PP. The surface area was also found to increase in PVC, which appeared to have formed crevices and pits after treatment KHE (Fig. 5, 6). These changes might be due to the corrosive effect of KOH, but further investigation is needed to confirm our observations (Karami et al. 2017). Nevertheless, the surface modification of PP and PVC was considered negligible in their identification using Raman spectroscopy, given the very high similarity between the Raman spectra before and after treatment KHE, i.e. 99% and 95%, respectively (Fig. 7; Table 5). Surface modification was not observed in the other types of microplastics after treatment KHE, whose Raman spectra before and after treatment were 94–99% similar (Fig. 7; Table 5).

An automated Raman mapping approach to identify microplastics

Treatment KHE was proven to be an effective approach to extract microplastics from seafood samples. The soft tissue of *P. viridis* and whole fish of *T. japonicus* including bones were used for demonstration, where microplastics were isolated on stainless-steel filter membranes and were identified using a Raman mapping technique (Fig. 8). This automated approach represents a great advance from the conventional time-consuming visual assessment and point acquisition approach to assess particles one by one, a method that is prone to handling errors, particularly for particles < 250 μm.

The resolution of Raman spectrometry can theoretically detect microplastics as small as 1–2 μm, while recent research has further improved this size detection limit to 0.1 μm (Sobhani et al., 2019, 2020; Xu et al., 2019; Levermore et al., 2020). However, a higher resolution is associated with a longer analysis time and therefore the areas of interest were usually small in the evaluation of Raman mapping methods (e.g. 88 μm × 88 μm in Sobhani et al. 2019, at 1 μm per pixel). It could be challenging to apply these high-resolution techniques in the environmental or food assessment of microplastics, given the increasing difficulty to isolate smaller-sized particles from the environmental or biological matrices and that the filter membranes could be easily clogged during the microplastic extraction process. In this connection, our goal is to develop a

Raman mapping approach that is more suitable for routine monitoring purposes. In the present study, a spatial resolution of 28.4 μm was used to target microplastics > 30 μm. With this resolution, the scanned area was increased to 8,000 μm × 8,000 μm and that the analysis time was controlled to about 14 h, which can be automatically run overnight to maximise productivity. However, certainly there are more advanced Raman or FTIR spectroscopes available in the market which can complete the same area of mapping in a shorter period of time. The actual protocol and analysis time should therefore be adjusted according to the ease of accessibility to equipment and the target size range of microplastics.

Another concern is that stainless-steel filter membranes, the proposed Raman substrate, usually do not have a homogenous surface (e.g. the plain Dutch weave pattern in Fig. 10a), and that the point of focus may not be stable on the target particles during the Raman mapping process. This problem is more pronounced at a higher magnification, but can probably be solved by the auto-focus function available in some Raman spectroscopes. In the present study, a low-magnification (10×) objective was used to address the concern, and the results were found satisfactory for identifying microplastics > 30 μm. With this automated Raman mapping approach, our findings revealed the presence of microplastics in Hong Kong waters, where *P. viridis* contained > 17 times more microplastics than *T. japonicus* per unit wet weight (Fig. 9a). This could be attributed to the filter-feeding nature of mussels, which makes them more susceptible than fish to ingestion of suspended particles during the feeding process (Li et al., 2019). Nevertheless, the microplastics determined in *P. viridis* and *T. japonicus* both displayed a similar size range of up to 820 μm and were dominated by PP and PE fragments (Fig. 9b–10).

In summary, this study addressed some major technical concerns in microplastic analysis in seafood by developing improved methods for biomass digestion, extraction of microplastics and their characterisation using an automated approach of Raman mapping. Our protocol is applicable to other biological samples and provides an improved alternative to streamline the workflow of microplastic analysis for routine monitoring purposes.

Acknowledgments

This study was supported by an internal research grant (P0001274) at The Hong Kong Polytechnic University. The authors acknowledge the University Research Facility in Chemical and Environmental Analysis, and the University Research Facility in Materials Characterisation and Device Fabrication, at The Hong Kong Polytechnic University for their technical assistance in Raman spectroscopy, 3D laser scanning microscopy, and scanning electron microscopy.

References

Andrady, A. L., 2011. Microplastics in the marine environment. Mar. Pollut. Bull. 62, 1596-1605.

Avio, C. G., Gorbi, S., Regoli, F., 2015. Experimental development of a new protocol for extraction and characterization of microplastics in fish tissues: First observations in commercial species from Adriatic Sea. Mar. Environ. Res. 111, 18-26.

Bagheri, T., Gholizadeh, M., Abarghouei, S., Zakeri, M., Hedayati, A., Rabaniha, M., Aghaeimoghadam, A., Hafezieh, M., 2020. Microplastics distribution, abundance and composition in sediment, fishes and benthic organisms of the Gorgan Bay, Caspian sea. Chemosphere 257, 127201.

612 Bancroft, J. D., Gamble, M., 2008. Theory and Practice of Histological Techniques (sixth ed.),
613 Churchill Livingstone, China, 725 pp.
614 Bonello, G., Varrella, P., Pane, L., 2018. First evaluation of microplastic content in benthic filter-
615 feeders of the Gulf of La Spezia (Ligurian Sea). J. Aquat. Food Prod. Technol. 27, 284-
616 291.
617 Castro, K., de Vallejuelo, S. F. O., Astondoa, I., Goñi, F. M., Madariaga, J. M. 2011. Analysis of
618 confiscated fireworks using Raman spectroscopy assisted with SEM- EDS and FTIR. J.
619 Raman Spectrosc. 42, 2000-2005.
620 Cho, Y., Shim, W. J., Jang, M., Han, G. M., Hong, S. H., 2019. Abundance and characteristics of
621 microplastics in market bivalves from South Korea. Environ. Pollut. 245, 1107-1116.
622 Claessens, M., Van Cauwenberghe, L., Vandegehuchte, M. B., Janssen, C. R., 2013. New
623 techniques for the detection of microplastics in sediments and field collected organisms.
624 Mar. Pollut. Bull. 70, 227-233.
625 Collard, F., Gilbert, B., Compère, P., Eppe, G., Das, K., Jauniaux, T., Parmentier, E., 2017.
626 Microplastics in livers of European anchovies (*Engraulis encrasicolus*, L.). Environ.
627 Pollut. 229, 1000-1005.
628 de Sá, L. C., Luís, L. G., Guilhermino, L., 2015. Effects of microplastics on juveniles of the
629 common goby (*Pomatoschistus microps*): Confusion with prey, reduction of the
630 predatory performance and efficiency, and possible influence of developmental
631 conditions. Environ. Pollut. 196, 359-362.
632 Dehaut, A., Cassone, A. L., Frère, L., Hermabessiere, L., Himber, C., Rinnert, E., Rivière, G.,
633 Lambert, C., Soudant, P., Huvet, A., Duflos, G., Paul-Pont, I., 2016. Microplastics in
634 seafood: Benchmark protocol for their extraction and characterization. Environ. Pollut.
635 215, 223-233.
636 Directive, S. F., 2013. Guidance on monitoring of marine litter in European Seas.
637 Garnier, Y., Jacob, H., Guerra, A. S., Bertucci, F., Lecchini, D., 2019. Evaluation of microplastic
638 ingestion by tropical fish from Moorea Island, French Polynesia. Mar. Pollut. Bull. 140,
639 165-170.
640 Gündoğdu, S., Çevik, C., Ataş, N. T., 2020. Stuffed with microplastics: Microplastic occurrence
641 in traditional stuffed mussels sold in the Turkish market. Food Biosci. 37, 100715.
642 Hermabessiere, L., Paul-Pont, I., Cassone, A. L., Himber, C., Receveur, J., Jezequel, R., Rakwe,
643 M. E., Rinnert, E., Rivière, G., Lambert, C., Huvet, A., Dehaut, A., Duflos, G., Soudant,
644 P., 2019. Microplastic contamination and pollutant levels in mussels and cockles
645 collected along the channel coasts. Environ. Pollut. 250, 807-819.
646 Hossain, M. S., Rahman, M. S., Uddin, M. N., Sharifuzzaman, S. M., Chowdhury, S. R., Sarker,
647 S., Chowdhury, M. S. N., 2020. Microplastic contamination in Penaeid shrimp from the
648 Northern Bay of Bengal. Chemosphere, 238, 124688.
649 James, K., Vasant, K., Padua, S., Gopinath, V., Abilash, K. S., Jeyabaskaran, R., Babu, A., John,
650 S., 2020. An assessment of microplastics in the ecosystem and selected commercially
651 important fishes off Kochi, south eastern Arabian Sea, India. Mar. Pollut. Bull. 154,
652 111027.
653 Jovanović, B., 2017. Ingestion of microplastics by fish and its potential consequences from a
654 physical perspective. Integr. Environ. Assess. Manag. 13, 510-515.
655 Karami, A., Golieskardi, A., Choo, C. K., Romano, N., Ho, Y. B., Salamatinia, B., 2017. A high-
656 performance protocol for extraction of microplastics in fish. Sci. Total Environ. 578, 485-
657 494.

Karbalaei, S., Golieskardi, A., Hamzah, H. B., Abdulwahid, S., Hanachi, P., Walker, T. R., Karami, A., 2019. Abundance and characteristics of microplastics in commercial marine fish from Malaysia. Mar. Pollut. Bull. 148, 5-15.

Katija, K., Choy, C. A., Sherlock, R. E., Sherman, A. D., Robison, B. H., 2017. From the surface to the seafloor: How giant larvaceans transport microplastics into the deep sea. Sci. Adv., 3, e1700715.

Kim, S. M., Kim, H., Lee, W. C., Kim, H. C., Lee, H., Kwak, S. N., Jo, N., Lee, S. H., 2016. Monthly variation in the proximate composition of jack mackerel (*Trachurus japonicus*) from Geumo Island, Korea. Fish. Res. 183, 371-378.

Käppler, A., Fischer, D., Oberbeckmann, S., Schernewski, G., Labrenz, M., Eichhorn, K.-J, Voit, B., 2016. Analysis of environmental microplastics by vibrational microspectroscopy: FTIR, Raman or both? Anal. Bioanal. Chem. 408, 8377-8391.

Lankers, M., 2019. Applications in: Environmental analytics (fine particles). Physical Sciences Reviews, 4.

Levermore, J.M., Smith, T.E.L., Kelly, F.J., Wright, S.L., 2020. Detection of microplastics in ambient particulate matter using Raman spectral imaging and chemometric analysis. Anal. Chem. 92, 8732-8740.

Li, J., Lusher, A. L., Rotchell, J. M., Deudero, S., Turra, A., Bråte, I. L. N., Sun, C., Hossainm M. S., Li, Q., Kolandhasamy, P., & Shi, H., 2019. Using mussel as a global bioindicator of coastal microplastic pollution. Environ. Pollut. 244, 522-533.

Lusher, A. L., Welden, N. A., Sobral, P., & Cole, M., 2017. Sampling, isolating and identifying microplastics ingested by fish and invertebrates. Anal. Methods 9, 1346-1360.

Löder, M.G.J., Kuczera, M., Mintenig, S., Lorenz, C., Gerdts, G., 2015. Focal plane array detector-based micro-Fourier-transform infrared imaging for the analysis of microplastics in environmental samples. Environ. Chem. 12, 563-581.

Nakajima, R., Yamashita, R., 2020 Methods for sampling, processing, identification, and quantification of microplastics in the marine environment. Oceanography in Japan, 29, 129-151 (in Japanese).

Nie, H., Wang, J., Xu, K., Huang, Y., Yan, M., 2019. Microplastic pollution in water and fish samples around Nanxun Reef in Nansha Islands, South China Sea. Sci. Total Environ. 696, 134022.

Oßmann, B. E., Sarau, G., Schmitt, S. W., Holtmannspötter, H., Christiansen, S. H., Dicke, W., 2017. Development of an optimal filter substrate for the identification of small microplastic particles in food by micro-Raman spectroscopy. Anal. Bioanal. Chem. 409, 4099-4109.

Phuong, N. N., Zalouk-Vergnoux, A., Kamari, A., Mouneyrac, C., Amiard, F., Poirier, L., & Lagarde, F., 2018. Quantification and characterization of microplastics in blue mussels (*Mytilus edulis*): Protocol setup and preliminary data on the contamination of the French Atlantic coast. Environ. Sci. Pollut. Res. 25, 6135-6144.

Plastics Europe. Plastics- The Facts. 2019. An analysis of European plastics production, demand and waste data.

Qiu, Q., Tan, Z., Wang, J., Peng, J., Li, M., Zhan, Z., 2016. Extraction, enumeration and identification methods for monitoring microplastics in the environment. Estuar. Coast Shelf Sci. 176, 102-109.

Qu, X., Su, L., Li, H., Liang, M., Shi, H., 2018. Assessing the relationship between the abundance and properties of microplastics in water and in mussels. Sci. Total Environ. 621, 679-686.

Roch, S., Brinker, A., 2017. Rapid and efficient method for the detection of microplastic in the gastrointestinal tract of fishes. Environ. Sci. Technol. 51, 4522-4530.

Sathish, M. N., Jeyasanta, K. I., Patterson, J., 2020. Monitoring of microplastics in the clam *Donax cuneatus* and its habitat in Tuticorin coast of Gulf of Mannar (GoM), India. Environ. Pollut. 266, 115219.

Sobhani, Z., Amin, M.A., Naidu, R., Megharaj, M., Fang, C., 2019. Identification and visualisation of microplastics by Raman mapping. Anal. Chem. Acta 1077, 191-199.

Sobhani, Z., Zhang, X., Gibson, C., Naidu, R., Megharaj, M., Fang, C., 2020. Identification and visualisation of microplastics/nanoplastics by Raman mapping (i): down to 100 nm. Water Res. 174, 115658.

Stuart B.H., 2002. Polymer Analysis. John Wiley and Sons, Chichester, 304 pp.

Sun, R., Yu, J., Liao, Y., Chen, J., Wu, Z., Mai, B., 2020. Geographical distribution and risk assessment of dichlorodiphenyltrichloroethane and its metabolites in *Perna viridis* mussels from the northern coast of the South China Sea. Mar. Pollut. Bull. 151, 110819.

Teng, J., Wang, Q., Ran, W., Wu, D., Liu, Y., Sun, S., Liu, H., Cao, R., Zhao, J., 2019. Microplastic in cultured oysters from different coastal areas of China. Sci. Total Environ. 653, 1282-1292.

Thiele, C. J., Hudson, M. D., Russell, A. E., 2019. Evaluation of existing methods to extract microplastics from bivalve tissue: Adapted KOH digestion protocol improves filtration at single-digit pore size. Mar. Pollut. Bull. 142, 384-393.

Tuschel, D., 2016. Selecting an excitation wavelength for Raman spectroscopy.

Van Cauwenberghe, L., Janssen, C. R., 2014. Microplastics in bivalves cultured for human consumption. Environ. Pollut. 193, 65-70.

Van Cauwenberghe, L., Claessens, M., Vandegehuchte, M. B., Janssen, C. R., 2015. Microplastics are taken up by mussels (*Mytilus edulis*) and lugworms (*Arenicola marina*) living in natural habitats. Environ. Pollut. 199, 10-17.

Verlaan, M. P., Banta, G. T., Khan, F. R., Syberg, K., 2019. Abundance of microplastics in the gastrointestinal tracts of the eelpout (*Zoacres viviparous* L.) collected in Roskilde Fjord, Denmark: Implications for use as a monitoring species under the Marine Strategy Framework Directive. Reg. Stud. Mar. Sci. 32, 100900.

Wobbrock, J. O., Findlater, L., Gergle, D., Higgins, J. J., 2011. The aligned rank transform for nonparametric factorial analyses using only anova procedures. In *Proceedings of The SIGCHI Conference on Human Factors in Computing Systems*. pp. 143-146.

Xiong, X., Zhang, K., Chen, X., Shi, H., Luo, Z., Wu, C., 2018. Sources and distribution of microplastics in China's largest inland lake–Qinghai Lake. Environ. Pollut. 235, 899-906.

Xu, J.L., Thomas, K.V., Luo, Z., Gowen, A.A., 2019. FTIR and Raman imaging for microplastics analysis: state of the art, challenges and prospects. Trends Anal. Chem. 119, 115629.

Zhang, X., Yan, B., Wang, X., 2020. Selection and optimization of a protocol for extraction of microplastics from *Mactra veneriformis*. Sci. Total Environ. 746, 141250.

Highlights

- An improved method to extract microplastics from organic and inorganic biomass
- An automated mapping approach to characterise the extracted microplastics
- The protocol for seafood also applicable to other biological samples